



Article

Antibacterial Activity of TiO₂- and ZnO-Decorated with Silver Nanoparticles

Van Thang Nguyen¹, Viet Tien Vu¹, The Huu Nguyen¹, Tuan Anh Nguyen², Van Khanh Tran³ and Phuong Nguyen-Tri^{4,*} 

¹ Faculty of Chemical Technology, Hanoi University of Industry, BacTu Liem, Hanoi 100000, Vietnam; thangnv2000@me.com (V.T.N.); vuviet.tphn@gmail.com (V.T.V.); nguyenthehuu@hau.edu.vn (T.H.N.)

² Institute for Tropical Technology, Vietnam Academy of Science and Technology, Hanoi 122100, Vietnam; ntanh2007@gmail.com

³ Hanvet Pharmaceutical and Veterinary Materials JSC, Hungyen17000, Vietnam; trankhanhhus@gmail.com

⁴ Department of Chemistry, University of Montreal, Montreal, QC H3T 1J4, Canada

* Correspondence: phuong.nguyen.tri@umontreal.ca; Tel.: +514-340-5121 (ext. 7326)

† Département de chimie, biochimie et physique, Université du Québec à Trois-Rivières, Trois-Rivières, QC G8Z 4M3, Canada.

Received: 23 May 2019; Accepted: 9 June 2019; Published: 17 June 2019



Abstract: This work emphasizes the use of the silver decorative method to enhance the antibacterial activity of TiO₂ and ZnO nanoparticles. These silver-decorated nanoparticles (hybrid nanoparticles) were synthesized using sodium borohydride as a reducing agent, with the weight ratio of Ag precursors/oxide nanoparticles = 1:30. The morphology and optical properties of these hybrid nanoparticles were investigated using transmission electron microscopy (TEM), X-ray diffraction (XRD) patterns, and UV-Vis spectroscopy. The agar-well diffusion method was used to evaluate their antibacterial activity against both *Staphylococcus aureus* and *Escherichia coli* bacteria, with or without light irradiation. The TEM images indicated clearly that silver nanoparticles (AgNPs, 5–10 nm) were well deposited on the surface of nano-TiO₂ particles (30–60 nm). In addition to this, bigger AgNPs (<20 nm) were dispersed on the surface of nano-ZnO particles (30–50 nm). XRD patterns confirmed the presence of AgNPs in both Ag-decorated TiO₂ and Ag-decorated ZnO nanoparticles. UV-Vis spectra confirmed that the hybridization of Ag and oxide nanoparticles led to a shift in the absorption edge of oxide nanoparticles to the lower energy region (visible region). The antibacterial tests indicated that both oxide pure nanoparticles did not exhibit inhibitory effects against bacteria, with or without light irradiation. However, the presence of AgNPs in their hybrids, even at low content (<40 mg/mL), leads to a good antibacterial activity, and higher inhibition zones under light irradiation as compared to those in dark were observed.

Keywords: silver nanoparticles; nano-TiO₂; nano-ZnO; nanohybrids; antibacterial

1. Introduction

It was reported in literature that nanoparticles can attack bacteria through six main mechanisms [1–15]: (i) destruction of the cell wall and peptidoglycan layer; (ii) release of toxic ions; (iii) destruction of protons efflux pumps and modification of membrane charges; (iv) formation of reactive oxygen species (ROS) degrading cell wall; (v) reactive oxygen species (ROS) degrading DNA, RNA, and proteins; and (vi) low adenosine triphosphate (ATP) production. In the case of metallic oxide nanoparticles (such as NiO, Co₃O₄, ZnO, Fe₂O₃, Fe₃O₄, MgO, CuO, TiO₂, and SiO₂), ROS is the predominant antibacterial mechanism, especially for nano-ZnO and nano-TiO₂. For noble metal nanoparticles, such as silver nanoparticles (AgNPs), they can attack effectively against

both *Gram-negative* and *Gram-positive* bacteria [16–19] via all six abovementioned antimicrobial mechanisms [20–22]. Therefore, in this application, AgNPs can be used as the sole antimicrobial agent. AgNPs could also react with bacteria through the photocatalytic production of ROS in solution [23]. However, Ag⁺-free ions released from AgNPs are considered toxic not only to human cells but also to the environment. Loading (embedding/immobilizing) AgNPs into oxide matrices is a new approach due to its ability to control solubility and toxicity of AgNPs. Various metallic oxide matrices have been used for loading/hybridizing AgNPs, such SiO₂, ZrO₂, Al₂O₃, Fe₃O₄, and CuO [24].

In the case of ZnO and TiO₂ nanoparticles, they can kill bacteria mainly through the ROS mechanism in the presence of UV light. The practical applications of these semiconducting oxide nanoparticles are limited due to the following two reasons: (i) wide band gap ~3.2 eV for nano-TiO₂ [25] and 3.37 eV for nano-ZnO [26] and (ii) high recombination of photogenerated electron–hole pairs [27–29]. Thus, two main approaches have been tried to improve the photocatalytic properties of these nanoparticles: (1) diminution of the recombination for photogenerated electron–hole pairs and (2) enhancement of the visible light sensitivity [25]. The first pathway focused on the design of heterostructures (heterojunctions) for these semiconducting oxide nanoparticles [30–34]. The formation of the Schottky barriers at the interface of noble metals/semiconducting oxide nanoparticles could significantly enhance the segregation of charges and helps to reduce the charge recombination [35,36]. For this reason, under UV irradiation, Ag-doped TiO₂ layers exhibited higher antibacterial activity against *Pseudomonas aeruginosa* bacteria compared to pure TiO₂ layers [37]. It is reported that the sensibility of TiO₂ with visible light could be significantly enhanced by doping with various elements [38,39].

Recently, the hybridization of noble metals (Au, Ag, Pd) and semiconducting oxides has become the most promising strategy to defeat the large band gap of semiconducting oxides [40–44]. The energy level alignment is combined by the heterojunction at the nanoscale in these nanoparticles. We have also recently published several books and articles on related topics [21,40,45,46].

In this study, the hybridization of AgNPs and ZnO/TiO₂ nanoparticles is expected not only to simply combine properties of single components, but also to significantly enhance their antibacterial properties [46]. Thus, this work aimed to investigate the role of silver decoration in enhancing the antibacterial activity of ZnO and TiO₂ nanoparticles against *Staphylococcus aureus* (ATCC 25923, Gram-positive) and *Escherichia coli* (Gram-negative, ATCC 25922).

2. Materials and Methods

2.1. Materials

TiO₂ (rutile) and ZnO nanoparticles were purchased from Sigma Aldrich (Singapore), having a mean diameter of <100 nm and a specific surface area of 18 and 15–25 m²/g, respectively. AgNO₃ and NaBH₄ were provided by Sigma Aldrich (Pathumwan, Bangkok, Thailand).

2.2. Synthesis of Silver-Decorated Nanoparticles

Firstly, 0.2 g of TiO₂ (or ZnO) nanoparticles was dispersed in 200 mL of distilled water under ultrasonication. AgNO₃ solution (0.01 g in 20 mL water) was then slowly added into the prepared nano-TiO₂ (or ZnO) solution under ultrasonication for 30 min. The mixing solution was then poured into the 500 mL three-necked pot. Then, NaBH₄ solution (0.01 g in 30 mL water) was added dropwise (1 drop/s) to the 500 mL three-necked pot. The reaction temperature was kept at 4 °C, and reaction mixture was stirred mechanically for 60 min. The nanohybrids were then collected by centrifugation at high speed (10,000 rpm) for 5 min. The residual precursors and agents were then fully removed after several rounds of centrifugation by adding fresh distilled water.

2.3. Characterization

The morphology of the hybrid nanoparticles was investigated using a transmission electron microscopy (JEM1010, JEOL, Tokyo, Japan), operating at 80 kV. UV-Vis spectra were obtained using a CINTRA 40 spectrophotometer (Cintra, Austin, TX, USA) in absorbance mode with 2 nm slit width. To verify the possible phases that were present in the Ag-decorated oxide nanoparticles, the X-ray diffraction method was used a Siemens D5000 diffractor (Siemens/Bruker, Aubrey, TX, USA) with $\text{CuK}\alpha$ radiation at the scan rate of $0.015^\circ \cdot \text{s}^{-1}$.

2.4. Antibacterial Tests

The agar-well diffusion method was used to evaluate antibacterial activity against Gram-positive (*Staphylococcus aureus*—ATCC 25923) and Gram-negative (*Escherichia coli*—ATCC 25922) bacteria. Nutrient agar plates were inoculated in brain heart infusion (BHI) broth using 100 μL of 106 CFU bacterial suspensions. Wells (8 mm diameter) were then punched in the inoculated plates using a sterile plastic rod. These wells were then filled with 50 μL of solution containing nanoparticles, at various concentrations, such as 8, 16, and 40 mg/mL. Control wells were filled with 50 μL of distilled water. These plates were the incubated at 37 $^\circ\text{C}$ for 18 h (with or without light irradiation). After this period, the antibacterial activities of these nanoparticles were evaluated by measuring the inhibition zone diameter around the wells (100 μm resolution; Model: Haloes Caliper—Zone Reader, IUL, Barcelone, Spain).

For the light irradiation test, LED (cold white, 1500 mcd, 3V DC) bulbs (two bulbs) were used with an illumination intensity of 300 lux. These cold white LEDs were designed by mixing blue (450–470 nm) and yellow (560–590 nm) lights that could be perceived by the naked eye as white color [46].

3. Results and Discussions

3.1. Characterization of Prepared Ag/TiO₂ and Ag/ZnO Nanoparticles

Figure 1 shows the electron microscopy images of AgNP-decorated nano-TiO₂ particles. As can be seen in this figure, AgNPs (black particles, 5–10 nm) were well dispersed on the surface of nano-TiO₂ particles (30–60 nm). The bigger nanoparticles are assigned to nano-TiO₂ and the smaller ones are AgNPs, as described in the literature [21]. It is worth noting that the synthesis process of hybrid nanoparticles was optimized to obtain the reported sizes of the hybrid nanoparticles.

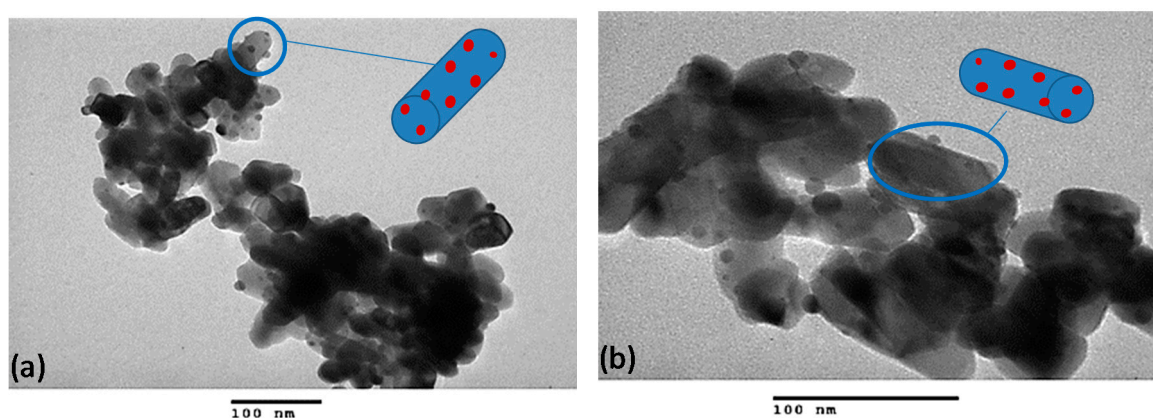


Figure 1. TEM images of Ag-loaded TiO₂ nanoparticles at different magnifications showing the hybrid structure; (a) 40,000 \times and (b) 80,000 \times . Inserted images show the schematic illustration of hybrid nanoparticles. The red point represents Ag nanoparticles, and the blue support is nano-TiO₂.

TEM images of AgNP-decorated nano-ZnO particles are shown in Figure 2. As shown in this figure, AgNPs (black spots <20 nm) were alternatively deposited and linked to nano-ZnO nanoparticles (30–50 nm). The presence of AgNPs is proven by a sharp peak, located at 410 nm in the UV-vis spectra

for these Ag/ZnO nanohybrids. For a comparative study, the size of AgNPs deposited on the surface of TiO₂ nanoparticles was smaller than that on the surface of ZnO nanoparticles.

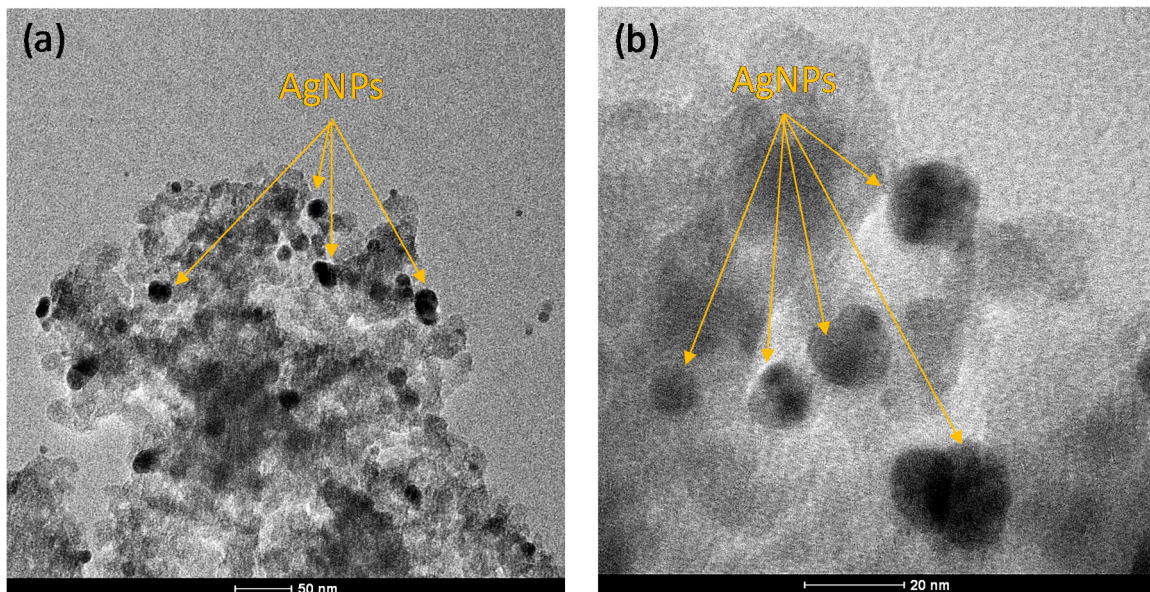


Figure 2. TEM images of Ag-loaded ZnO nanoparticles at different magnifications: (a) 43,000× and (b) 195,000×.

Figure 3 presents the XRD patterns of TiO₂ and Ag/TiO₂ nanoparticles. Figure 3a shows that the rutile phases of TiO₂ exhibit several diffraction peaks, and the reflections at (110), (101), (111), and (211) appear as the most intense, which is in line with the literature [47]. In the case of Ag/TiO₂ in Figure 3b, the intense peak at 38° refers to a (111) reflection of metallic Ag [48]. Due to low concentration (as compared to TiO₂ nanoparticles), other peaks of Ag are dominated by TiO₂ phases.

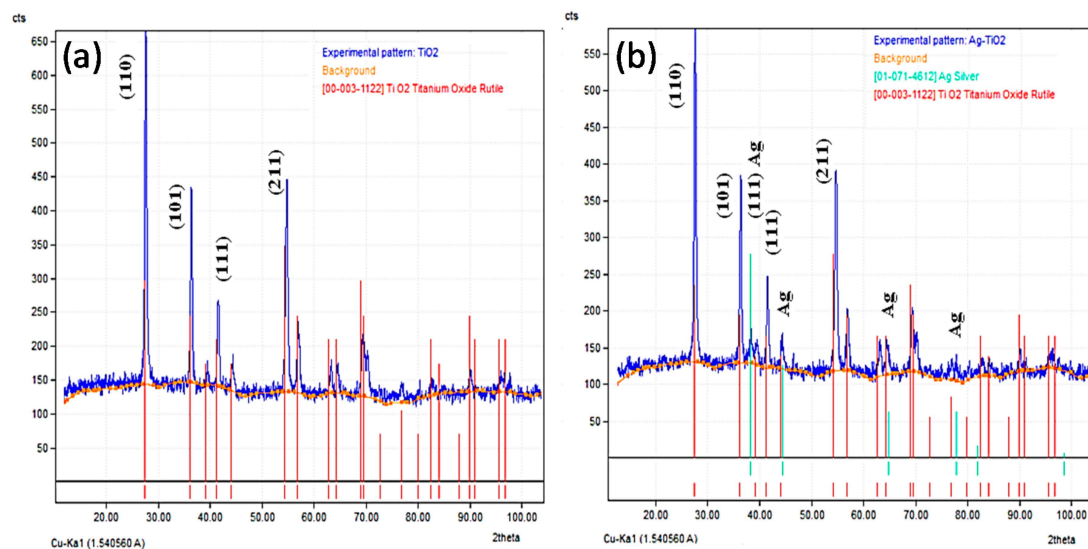


Figure 3. XRD patterns of (a) TiO₂ nanoparticles and (b) Ag/TiO₂ nanoparticles.

Figure 4 shows the XRD patterns of ZnO and Ag/ZnO nanoparticles. For the pure ZnO nanoparticles, all characteristics of the X-ray diffraction for ZnO are observed, especially the 100, 103, and 202 plans. In the case of ZnO-decorated with metallic Ag, some new peaks assigned to the (111), (200), (220), and (311) reflections are observed at high intensity [48,49]. This helps to confirm the presence of successful synthesis of these nanomaterials.

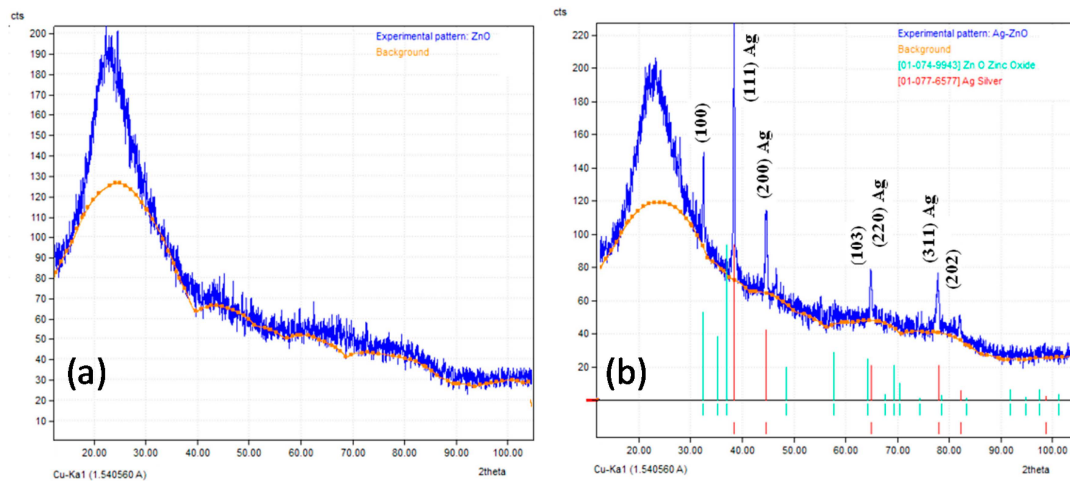


Figure 4. XRD patterns of (a) ZnO nanoparticles and (b) Ag/ZnO nanoparticles.

Figure 5 shows the UV-visible spectra of aqueous solutions containing AgNPs, TiO₂, and Ag/TiO₂ nanoparticles. In the case of AgNPs (~10 nm of diameter), a broad band around 398 nm is believed to be present due to the surface plasmon resonance (SPR peak) of AgNPs [50]. The absorption band for pure TiO₂ nanoparticles was observed in the UV region (at 360 nm), whereas it was shifted to the visible region for Ag-decorated TiO₂ nanoparticles. These results are in line with those reported in the literature for Ag-doped TiO₂ nanomaterials [51,52]. Figure 6 shows the UV-visible spectra for nano-ZnO- and nano-TiO₂-decorated with AgNPs (dispersed in water). This figure shows a broad band at the 410 nm band, indicating the presence of AgNPs on the surface of the nano-ZnO particles.

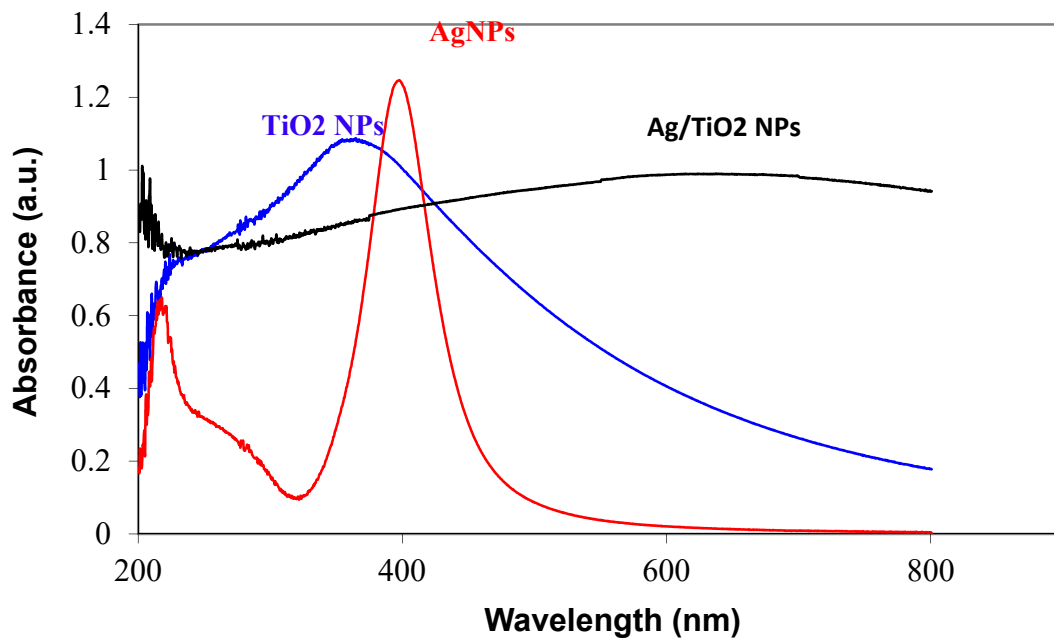


Figure 5. UV-Vis spectra of AgNPs, nano-TiO₂, and AgNP-decorated nano-TiO₂ particles (dispersed in water).

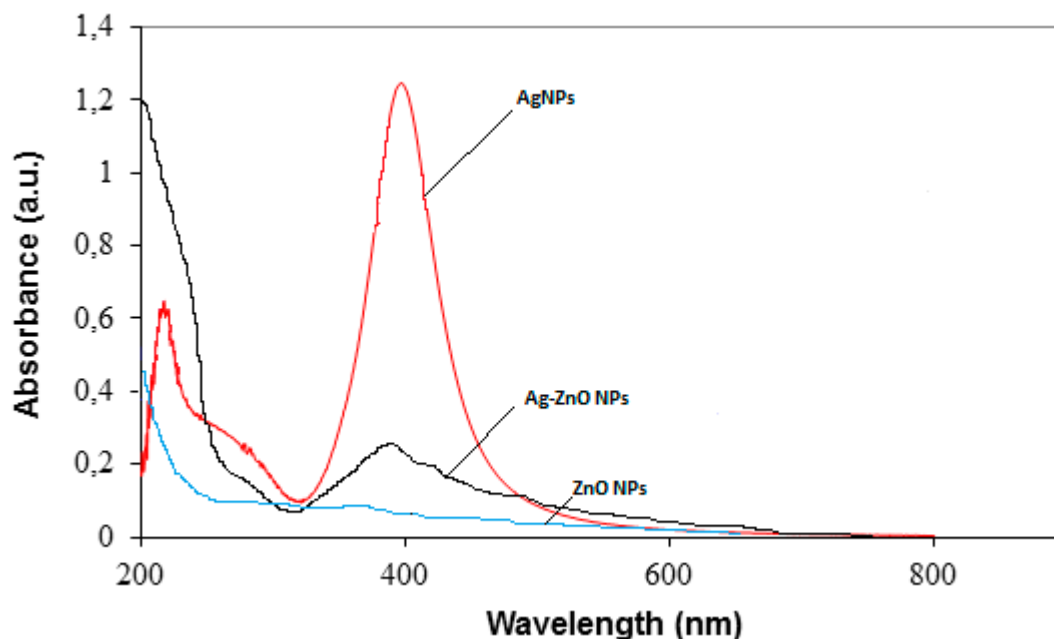


Figure 6. UV-Vis spectra of AgNP-decorated nano-ZnO particles (dispersed in water).

3.2. Antibacterial Tests

3.2.1. TiO₂ and Ag/TiO₂ Nanoparticles

Figures 7 and 8 present the photographs of antibacterial tests for nano-TiO₂ and Ag/TiO₂ NPs against *S. aureus* and *E. coli* bacteria, with and without light irradiation, respectively. Tables 1 and 2 show their corresponding inhibition zones. Figure 7a,b indicates that in the dark, TiO₂ NPs do not exhibit inhibitory effects to *S. aureus* bacteria (at concentrations of 10–40 mg/mL), whereas Ag-loaded TiO₂ NPs show a significant antibacterial activity at a concentration of 40 mg/mL. It was reported that TiO₂ nanoparticles are easy to attach to the cell membranes and accumulate [53–55]. In general, TiO₂ nanoparticles can destroy the pathogenic bacteria by the ROS mechanism under UV light radiation. Since the emitted wavelengths of the white LED lights include peaks in the blue (450–470 nm) and yellow (560–590 nm) areas, the inhibition zone of Ag-loaded TiO₂ NPs (40 mg/mL) could be attributed to the content of AgNPs in the nanohybrids (e.g., ~1.3 mg/mL). It is worth noting that the concentration of TiO₂ in nanohybrids is 30 times higher than that of AgNPs (from synthesis: the weight ratio of Ag precursors:TiO₂ = 1:30). These nanoparticles exhibited an inhibition zone of 2 mm (in diameter) at the lower concentration of 16 mg/mL, indicating the contribution of TiO₂ nanoparticles in these nanohybrids to their antibacterial activity (Table 1). At a concentration of 40 mg/mL, their inhibition zone is similar to that observed in the dark (4 mm in diameter), indicating the dominated contribution of AgNPs to the antibacterial activity.

Figure 7c,d shows that TiO₂ NPs did not exhibit inhibitory effects to bacteria under light irradiation (at concentration of 8–40 mg/mL). It was reported that the doping TiO₂ with noble metals shifted its absorption band to the visible region [40]. Without UV irradiation, pure TiO₂ nanoparticles did not inhibit bacterial growth. However, Ag–TiO₂ core–shell nanoparticles exhibited a good antibacterial activity against both *E. coli* and *S. aureus* bacteria without UV light [56,57]. Other authors have also reported that TiO₂ nanoparticles with highly dispersed Ag clusters are entirely restricted the growth of the *E. coli* bacterial [58]. Barudin et al. [59] indicated that Ag–TiO₂ nanoparticles exhibited superior antibacterial activity, as compared to pure TiO₂ nanoparticles, even under visible light irradiation [59].

In this work, for *E. coli* bacteria, under light irradiation, Ag/TiO₂ nanohybrids show a higher antibacterial activity than that in the dark. Table 2 shows that, in the dark, the inhibition zones of Ag/TiO₂ nanohybrids increase with their concentration, due to the increase of AgNP concentration in the nanohybrids.

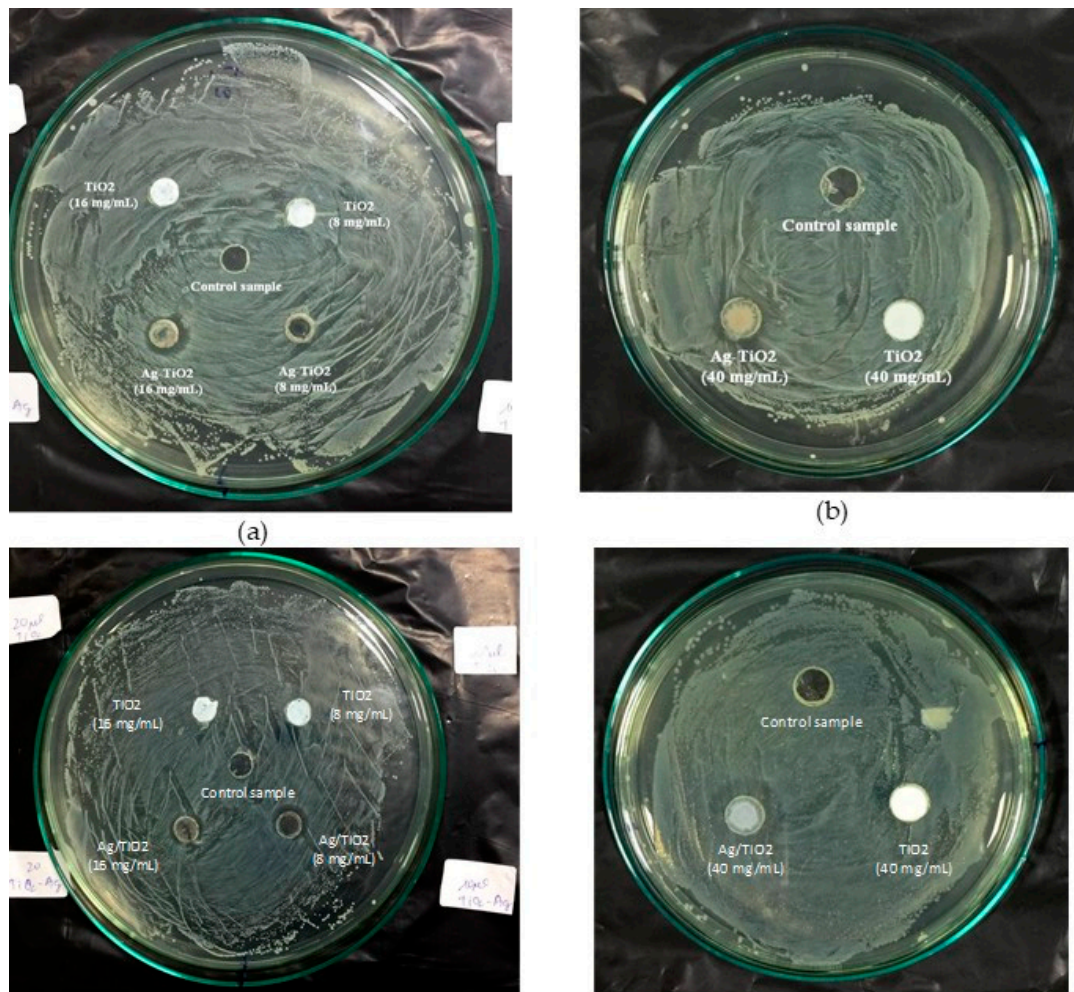


Figure 7. Photographs of antibacterial test against *Staphylococcus aureus* bacteria (agar-well diffusion method) for pure TiO₂ and Ag-loaded TiO₂ nanoparticles: (a) and (b): without light irradiation; (c) and (d): under light irradiation. Concentrations of AgNPs used are 8, 16, and 40 mg/mL.

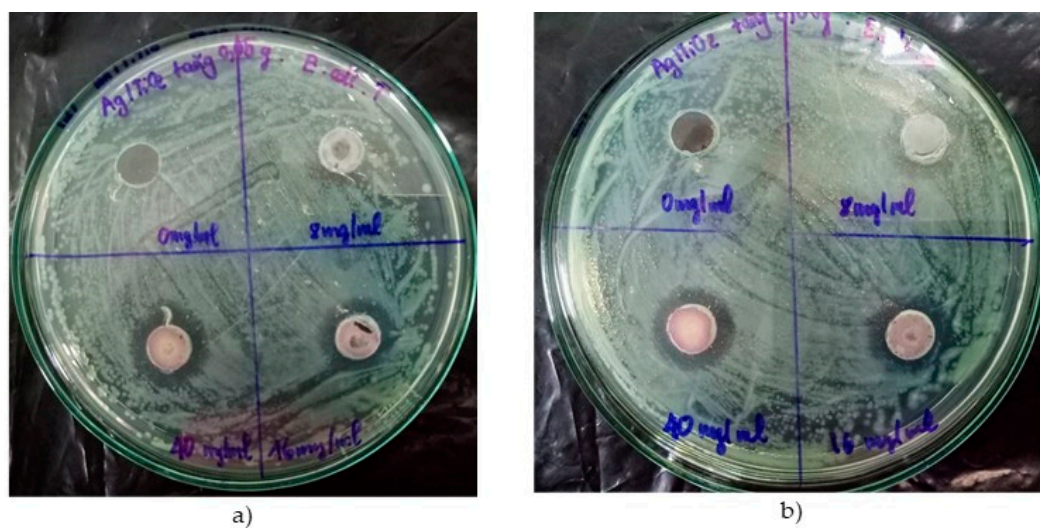


Figure 8. Photographs of antibacterial test against *Escherichia coli* bacteria (agar-well diffusion method) for Ag-loaded TiO₂ nanoparticles: (a) without light irradiation; (b) under light irradiation. Concentration of 8, 16, and 40 mg/mL.

Table 1. Antibacterial activity against *S. aureus* bacteria of TiO₂ nanoparticles and Ag-loaded TiO₂ nanoparticles.

Concentrations (mg/mL)	Inhibition Zone (mm)			
	Without Light Irradiation		Under Light Irradiation	
	TiO ₂ Nanoparticles	Ag-Decorated TiO ₂ Nanoparticles	TiO ₂ Nanoparticles	Ag-Decorated TiO ₂ Nanoparticles
8	0	0	0	0
16	0	0	0	2
40	0	4	0	4

Table 2. Antibacterial activity against *E. coli* bacteria of TiO₂ nanoparticles and Ag-loaded TiO₂ nanoparticles.

Concentrations (mg/mL)	Inhibition Zone (mm)			
	Without Light Irradiation		Under Light Irradiation	
	TiO ₂ Nanoparticles	Ag-Decorated TiO ₂ Nanoparticles	TiO ₂ Nanoparticles	Ag-Decorated TiO ₂ Nanoparticles
8	0	2	0	6
16	0	6	0	8
40	0	8	0	8

3.2.2. ZnO and Ag/ZnO Nanoparticles

It was reported in literature that ZnO has the inherent gain of broad antibacterial activities against virus, bacteria, fungus, and spores [60–62]. Stoimenov et al. [63] defined that ZnO nanoparticles attach on the bacterial surface due to electrostatic force of attraction. We expect that the hybridization of AgNPs with ZnO NPs may exhibit a superior antibacterial activity compared to their counterparts [45].

Figures 9 and 10 show the photographs of an antibacterial test for nano-ZnO and Ag/ZnO NPs against *S. aureus* and *E. coli* bacteria, without and with light irradiation, respectively. Tables 3 and 4 show their corresponding inhibition zones. Figures 9 and 10 indicate that ZnO NPs did not exhibit inhibitory effects for both bacteria, with or without light irradiation (at concentrations of 10–40 mg/mL).

For Ag/ZnO nanohybrids, as shown in Tables 3 and 4, light irradiation leads to an increase of the diameter of the inhibition zone for both *S. aureus* (at 8 mg/mL) and *E. coli* (at 8, 16, and 40 mg/mL) bacteria. Similarity, Ibanescu et al. [64] reported the antimicrobial property of Ag/ZnO nanocomposites against both *E. coli* and *M. luteus* bacteria. Their finding indicates that small amounts of silver could significantly enhance antimicrobial activity. The photocatalytic activity of Ag/ZnO nanocomposites could also contribute to enhancing antimicrobial activity. Nagaraju et al. [65] indicated an improvement of antimicrobial activity of Ag–ZnO NPs against both *E. coli* and *S. aureus* bacteria compared to pure materials. The inhibition zone could be observed at a concentration of 500 µg Ag–ZnO NPs. Wei et al. [66] also described the high antibacterial activity of Ag–ZnO hybrid nanofibers against *E. coli* and *P. aeruginosa* bacteria.

For the comparative study, under light irradiation at a low concentration (8 mg/mL), Ag/ZnO nanohybrids exhibit higher antibacterial activity against both two bacteria than Ag–Ag/TiO₂ nanohybrids. One possible explanation is the better hybridization between Ag and ZnO nanoparticles, through the presence of the SPR peak in Ag/ZnO nanoparticles (Figure 6), whereas the SPR peak seems to disappear in the Ag/TiO₂ nanoparticles (Figure 5).

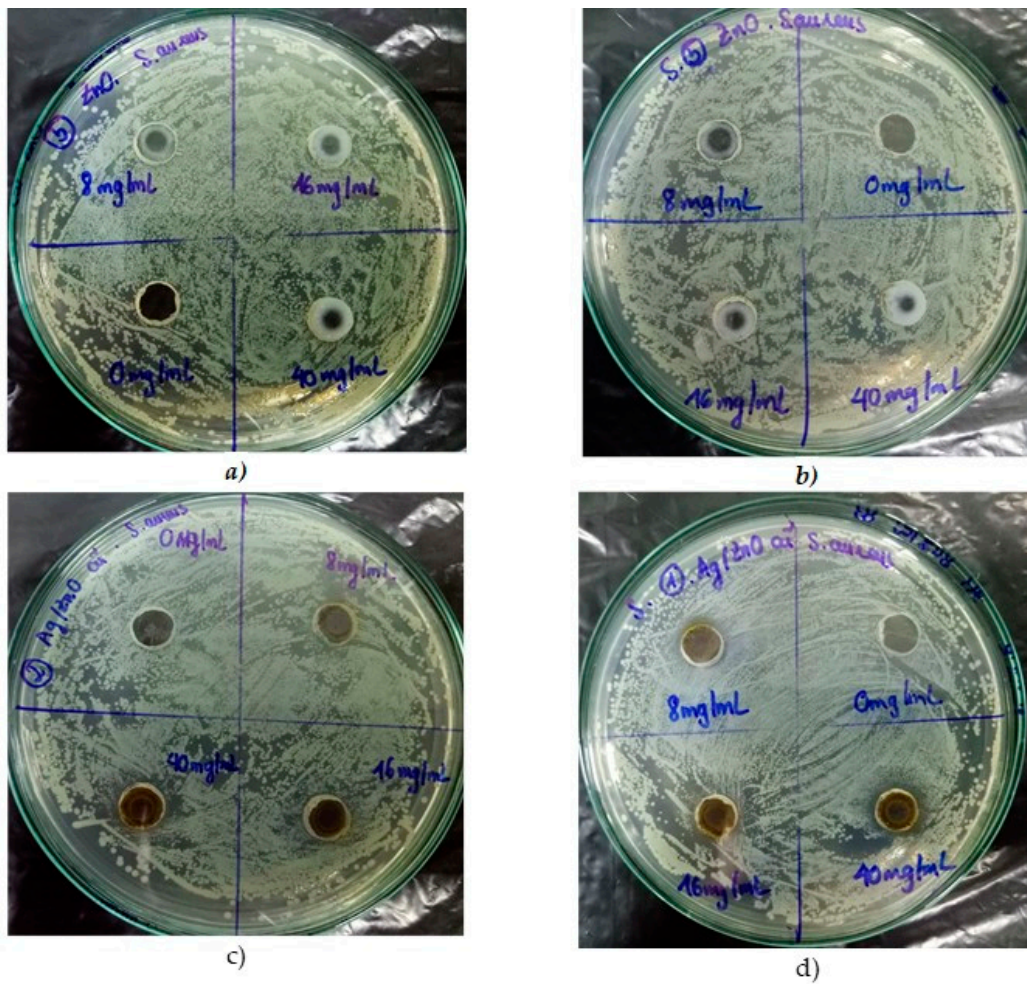


Figure 9. Photographs of antibacterial test against *S. aureus* bacteria (agar-well diffusion method) for pure ZnO nanoparticles ((a): without light irradiation; (b): under light irradiation) and Ag-loaded ZnO nanoparticles ((c): without light irradiation; (d): under light irradiation).

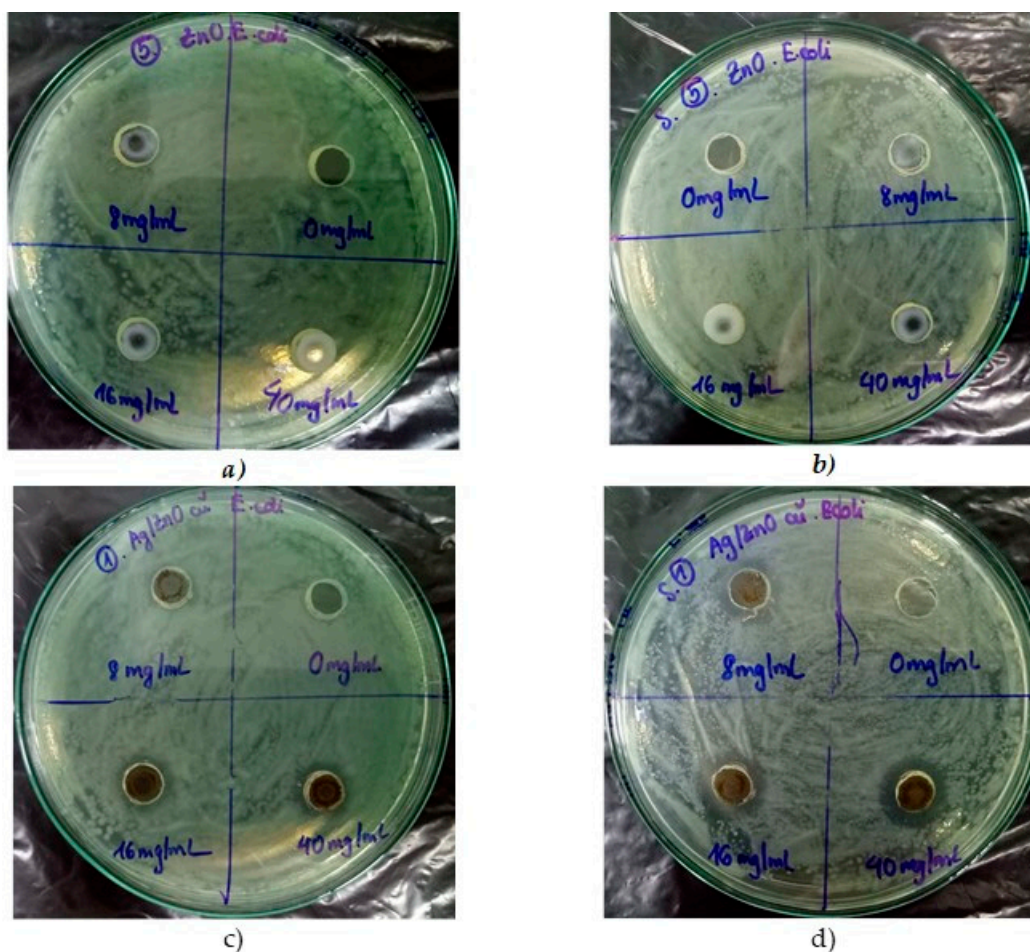


Figure 10. Photographs of antibacterial test against *E. coli* bacteria (agar-well diffusion method) for ZnO nanoparticles ((a): without light irradiation; (b): under light irradiation) and Ag-loaded ZnO nanoparticles ((c): without light irradiation; (d): under light irradiation).

Table 3. Antibacterial activity against *S. aureus* bacteria of ZnO nanoparticles and Ag-loaded ZnO nanoparticles.

Concentrations (mg/mL)	Inhibition Zone (mm)			
	Without Light Irradiation		With Light Irradiation	
	ZnO Nanoparticles	Ag-Decorated ZnO Nanoparticles	ZnO nanoparticles	Ag-Decorated ZnO Nanoparticles
8	0	0	0	2
16	0	2	0	2
40	0	4	0	4

Table 4. Antibacterial activity against *E. coli* bacteria of ZnO nanoparticles and Ag-loaded ZnO nanoparticles.

Concentrations (mg/mL)	Inhibition Zone (mm)			
	Without Light Irradiation		With Light Irradiation	
	ZnO Nanoparticles	Ag-Decorated ZnO Nanoparticles	ZnO Nanoparticles	Ag-Decorated ZnO Nanoparticles
8	0	2	0	7
16	0	4	0	8
40	0	6	0	8

4. Conclusions

This research is a continuous works focused on polymers and multifunctional composites [67–86]. The main findings of this work were as follows:

1. Silver-decorated oxide nanoparticles were successfully prepared using sodium borohydride as a reducing agent, with the weight ratio of Ag precursors:oxide nanoparticles = 1:30.
2. The TEM images indicated that AgNPs (5–10 nm) were deposited on the surface of nano-TiO₂ particles (30–60 nm), whereas the bigger AgNPs (<20 nm) were dispersed on the surface of nano-ZnO particles (30–50 nm). XRD patterns confirmed the presence of AgNPs in both Ag-decorated TiO₂ and Ag-decorated ZnO nanoparticles.
3. UV-vis spectra indicated that the hybridization of Ag and oxide nanoparticles led to a shift in the absorption edge of oxide nanoparticles to the lower energy region (visible region).
4. The antibacterial tests indicated that both oxide nanoparticles did not exhibit inhibitory against bacteria, with or without light irradiation. However, the presence of AgNPs in their hybrids (at a concentration <40 mg/mL) exhibited higher inhibition zones under light irradiation, as compared to that in dark. At a high concentration of 40 mg/mL, the antibacterial behavior of these nanohybrids under light irradiation is similar to that in dark, indicating the dominated contribution of AgNPs to the antibacterial activity of these nanohybrids (at this high concentration).
5. In the comparative study, under light irradiation at a low concentration (8 mg/mL), Ag/ZnO nanohybrids exhibited higher antibacterial activity against both bacteria than the Ag–Ag/TiO₂ nanohybrids.

Author Contributions: Conceptualization and methodology, P.N.-T., T.A.N. and V.T.N.; synthesis of ZnO–AgNPs, V.T.V., V.K.T. and V.T.N.; Synthesis of TiO₂–AgNPs, T.H.N. and V.K.T.; writing—original draft preparation, T.A.N.; writing—review and editing P.N.-T.; supervision, P.N.-T.

Funding: This work was financial supported by Natural Sciences and Engineering Research Council of Canada (NSERC).

Conflicts of Interest: The authors declare no conflict of interest.

References

1. Rai, V.R.; Bai, A.J. Nanoparticles and their potential application as antimicrobials. In *Science against microbial pathogens: Communicating current research and technological advances*, Formatex, Microbiology Series No.3; Méndez-Vilas, A., Ed.; Elsevier: Badajoz, Spain, 2011; Volume 1, pp. 97–209.
2. BECON. *Nanoscience and Nanotechnology Symposium Report*; National Institutes of Health Bioengineering Consortium: Bethesda, MD, USA, June 2000. Available online: <http://www.uta.edu/rfmems/060515-NSF-NUE/Info/biomed/nanotechsympreport.pdf> (accessed on 10 June 2019).
3. Rtimi, S.; Nadtochenko, V.; Khmel, I.; Konstantinidis, S.; Britun, N.; Kiwi, J. Monitoring the energy of the metal ion-content plasma-assisted deposition and its implication for bacterial inactivation. *Appl. Sur. Sci.* **2019**, *467*, 749–752. [[CrossRef](#)]
4. Oesterling, E.; Chopra, N.; Gavalas, V.; Arzuaga, X.; Lim, E.J.; Sultana, R.; Butterfield, D.A.; Bachas, L.; Hennig, B. Alumina nanoparticles induce expression of endothelial cell adhesion molecules. *Toxicol. Lett.* **2008**, *178*, 160–166. [[CrossRef](#)] [[PubMed](#)]
5. Dey, S.; Bakthavatchalu, V.; Tseng, M.T.; Wu, P.; Florence, R.L.; Grulke, E.A.; Yokel, R.A.; Dhar, S.K.; Yang, H.-S.; Chen, Y.; et al. Interactions between SIRT1 and AP-1 reveal a mechanistic insight into the growth promoting properties of alumina (Al₂O₃) nanoparticles in mouse skin epithelial cells. *Carcinogenesis* **2008**, *29*, 1920–1929. [[CrossRef](#)] [[PubMed](#)]
6. Chang, Y.-N.; Zhang, M.; Xia, L.; Zhang, J.; Xing, G. The Toxic Effects and Mechanisms of CuO and ZnO Nanoparticles. *Materials* **2012**, *5*, 2850–2871. [[CrossRef](#)]
7. Karlsson, H.L.; Cronholm, P.; Gustafsson, J.; Möller, L. Copper Oxide Nanoparticles Are Highly Toxic: A Comparison between Metal Oxide Nanoparticles and Carbon Nanotubes. *Chem. Res. Toxicol.* **2008**, *21*, 1726–1732. [[CrossRef](#)] [[PubMed](#)]

8. Xia, T.; Kovoichich, M.; Liong, M.; Mädler, L.; Gilbert, B.; Shi, H.; Yeh, J.I.; Zink, J.I.; Nel, A.E. Comparison of the Mechanism of Toxicity of Zinc Oxide and Cerium Oxide Nanoparticles Based on Dissolution and Oxidative Stress Properties. *ACS Nano* **2008**, *2*, 2121–2134. [[CrossRef](#)] [[PubMed](#)]
9. Rtimi, S.; Dionysiou, D.; Pillai, S.C.; Kiwi, J. Advances in catalytic/photocatalytic bacterial inactivation by nano Ag and Cu coated surfaces and medical devices. *Appl. Catal. B Environ.* **2019**, *240*, 291–318. [[CrossRef](#)]
10. Ren, G.; Hu, D.; Cheng, E.W.; Vargas-Reus, M.A.; Reip, P.; Allaker, R.P. Characterisation of copper oxide nanoparticles for antimicrobial applications. *Int. J. Antimicrob. Agents* **2009**, *33*, 587–590. [[CrossRef](#)] [[PubMed](#)]
11. Niskanen, J.; Shan, J.; Tenhu, H.; Jiang, H.; Kauppinen, E.; Barranco, V.; Picó, F.; Yliniemi, K.; Kontturi, K. Synthesis of copolymer-stabilized silver nanoparticles for coating materials. *Colloid Polym. Sci.* **2010**, *288*, 543–553. [[CrossRef](#)]
12. Guggenbichler, J.-P.; Böswald, M.; Lugauer, S.; Krall, T. A new technology of microdispersed silver in polyurethane induces antimicrobial activity in central venous catheters. *Infect* **1999**, *27*, S16–S23. [[CrossRef](#)]
13. Azam, A.; Ahmed, A.S.; Oves, M.; Khan, M.; Memic, A. Size-dependent antimicrobial properties of CuO nanoparticles against Gram-positive and -negative bacterial strains. *Int. J. Nanomed.* **2012**, *7*, 3527–3535. [[CrossRef](#)] [[PubMed](#)]
14. Allaker, R.P. The use of nanoparticles to control oral biofilm formation. *J. Dent. Res.* **2010**, *89*, 1175–1185. [[CrossRef](#)] [[PubMed](#)]
15. Santos, C.L.; Albuquerque, A.J.R.; Sampaio, F.C.; Keyson, D. Nanomaterials with Antimicrobial Properties: Applications in Health Sciences. In *Microbial Pathogens and Strategies for Combating Them: Science, Technology and Education*; Méndez-Vilas, A., Ed.; Formatex: Badajoz, Spain, 2013.
16. Huang, H.H.; Ni, X.P.; Loy, G.L.; Chew, C.H.; Tan, K.L.; Loh, F.C.; Deng, J.F.; Xu, G.Q. Photochemical Formation of Silver Nanoparticles in Poly(N-vinylpyrrolidone). *Langmuir* **1996**, *12*, 909–912. [[CrossRef](#)]
17. Weir, E.; Lawlor, A.; Whelan, A.; Regan, F. The use of nanoparticles in anti-microbial materials and their characterization. *Analyst* **2008**, *133*, 835–845. [[CrossRef](#)] [[PubMed](#)]
18. Marambio-Jones, C.; Hoek, E.M.V. A review of the antibacterial effects of silver nanomaterials and potential implications for human health and the environment. *J. Nanopart. Res.* **2010**, *12*, 1531–1551. [[CrossRef](#)]
19. Shenashen, M.A.; El-Safty, S.A.; Elshehy, E.A. Synthesis, morphological control, and properties of silver nanoparticles in potential applications. *Part. Part. Syst. Charact.* **2014**, *31*, 293–316. [[CrossRef](#)]
20. Li, Q.; Mahendra, S.; Lyon, D.Y.; Brunet, L.; Liga, M.V.; Li, D.; Alvarez, P.J. Antimicrobial nanomaterials for water disinfection and microbial control: Potential applications and implications. *Water Res.* **2008**, *42*, 4591–4602. [[CrossRef](#)]
21. Nguyen-Tri, P.; Nguyen, V.T.; Nguyen, T.A. Biological activity and nanostructuring of Fe₃O₄-Ag/polyethylene nanocomposites. *J. Compos. Sci.* **2019**, *3*. [[CrossRef](#)]
22. Hussain, S.M.; Hess, K.L.; Gearhart, J.M.; Geiss, K.T.; Schlager, J.J. In vitro toxicity of nanoparticles in BRL 3A rat liver cells. *Toxicol. Vitro.* **2005**, *19*, 975–983. [[CrossRef](#)]
23. Le Ouay, B.; Stellacci, F. Antibacterial activity of silver nanoparticles: A surface science insight. *Nano Today* **2015**, *10*, 339–354. [[CrossRef](#)]
24. Dhanalekshmi, K.; Van Thang Nguyen, I.; Magesan, P. Chapter 26: Nanosilver loaded oxide nanoparticles for antibacterial application. In *Smart Nanocontainers: Fundamentals and Emerging Applications*; Nguyen-Tri, P., Do, T.-O., Nguyen, T.A., Eds.; Elsevier: Amsterdam, The Netherlands, 2019; ISBN 9780128167700.
25. Akhavan, O. Lasting antibacterial activities of Ag-TiO₂/Ag/a-TiO₂ nanocomposite thin film photocatalysts under solar light irradiation. *J. Colloid Interface Sci.* **2009**, *336*, 117–124. [[CrossRef](#)] [[PubMed](#)]
26. Gholap, H.; Warule, S.; Sangshetti, J.; Kulkarni, G.; Banpurkar, A.; Satpute, S.; Patil, R. Hierarchical nanostructures of Au@ZnO: Antibacterial and antibiofilm agent. *Appl. Microbiol. Biotechnol.* **2016**, *100*, 5849–5858. [[CrossRef](#)] [[PubMed](#)]
27. Tamaki, Y.; Hara, K.; Katoh, R.; Tachiya, M. A Femtosecond visible-to-IR spectroscopy of TiO₂ nanocrystalline films: Elucidation of the electron mobility before deep trapping. *J. Phys. Chem. C* **2009**, *113*, 11741–11746. [[CrossRef](#)]
28. Chen, X.; Mao, S.S. Titanium Dioxide Nanomaterials: Synthesis, Properties, Modifications, and Applications. *Chem. Rev.* **2007**, *107*, 2891–2959. [[CrossRef](#)] [[PubMed](#)]
29. Kudo, A.; Miseki, Y. Heterogeneous photocatalyst materials for water splitting. *Chem. Soc. Rev.* **2009**, *38*, 253–278. [[CrossRef](#)] [[PubMed](#)]

30. Sun, L.; Li, J.; Wang, C.; Li, S.; Lai, Y.-K.; Chen, H.; Lin, C. Ultrasound aided photochemical synthesis of Ag loaded TiO₂ nanotube arrays to enhance photocatalytic activity. *J. Hazard. Mater.* **2009**, *171*, 1045–1050. [[CrossRef](#)] [[PubMed](#)]
31. Abdulla-Al-Mamun, M.; Kusumoto, Y.; Zannat, T.; Islam, M.S. Synergistic enhanced photocatalytic and photothermal activity of Au@TiO₂ nanopellets against human epithelial carcinoma cells. *Phys. Chem. Chem. Phys.* **2011**, *13*, 21026. [[CrossRef](#)] [[PubMed](#)]
32. Jang, J.S.; Choi, S.H.; Kim, H.G.; Lee, J.S. Location and State of Pt in Platinized CdS/TiO₂ Photocatalysts for Hydrogen Production from Water under Visible Light. *J. Phys. Chem. C* **2008**, *112*, 17200–17205. [[CrossRef](#)]
33. Sarkar, D.; Ghosh, C.K.; Mukherjee, S.; Chattopadhyay, K.K. Three dimensional Ag₂O/TiO₂ type-II (p-n) nanoheterojunctions for superior photocatalytic activity. *ACS Appl. Mater. Interfaces* **2013**, *5*, 331–337. [[CrossRef](#)]
34. Ji, Y.F.; Guo, W.; Chen, H.H.; Zhang, L.S.; Chen, S.; Hua, M.T.; Long, Y.H.; Chen, Z. Surface Ti₃₊/Ti₄₊ redox shuttle enhancing photocatalytic H₂ production in ultrathin TiO₂ nanosheets/CdSe quantum dots. *J. Phys. Chem. C* **2015**, *119*, 27053–27059. [[CrossRef](#)]
35. Deng, Q.; Tang, H.; Liu, G.; Song, X.; Xu, G.; Li, Q.; Ng, D.H.; Wang, G. The fabrication and photocatalytic performances of flower-like Ag nanoparticles/ZnO nanosheets-assembled microspheres. *Appl. Surf. Sci.* **2015**, *331*, 50–57. [[CrossRef](#)]
36. Liang, Y.M.; Guo, N.; Li, L.L.; Li, R.Q.; Ji, G.J.; Gan, S.C. Fabrication of porous 3D flower-like Ag/ZnO heterostructure composites with enhanced photocatalytic performance. *Appl. Surf. Sci.* **2015**, *332*, 32–39. [[CrossRef](#)]
37. Ubonchonlakate, K.; Sikong, L.; Saito, F.P. aeruginosa inactivation with silver and nickel doped TiO₂ films coated on glass fiber roving. *Adv. Mater. Res.* **2011**, *150–151*, 1726–1731.
38. Umebayashi, T.; Yamaki, T.; Tanaka, S.; Asai, K. Visible light-induced degradation of methylene blue on S-doped TiO₂. *Chem. Lett.* **2003**, *32*, 330–331. [[CrossRef](#)]
39. Pelaez, M.; Nolan, N.T.; Pillai, S.C.; Seery, M.K.; Falaras, P.; Kontos, A.G.; Dunlop, P.S.M.; Hamilton, J.W.J.; Byrne, J.A.; O'Shea, K.; et al. A Review on the Visible Light Active Titanium Dioxide Photocatalysts for Environmental Applications. *Appl. Catal. B Environ.* **2012**, *125*, 331–349. [[CrossRef](#)]
40. Mohapatra, S.; Nguyen, T.A.; Nguyen-Tri, P. *Noble Metal-Metal Oxide Hybrid Nanoparticles: Fundamentals and Applications*; Elsevier: Amsterdam, The Netherlands, 2018; Volume 1.
41. Fageria, P.; Gangopadhyay, S.; Pande, S. Synthesis of ZnO/Au and ZnO/Ag nanoparticles and their photocatalytic application using UV and visible light. *RSC Adv.* **2014**, *4*, 24962–24972. [[CrossRef](#)]
42. Xu, C.; Chen, P.; Liu, J.; Yin, H.; Gao, X.; Mei, X. Fabrication of visible-light-driven Ag/TiO₂ heterojunction composites induced by shock wave. *J. Alloy. Compd.* **2016**, *679*, 463–469. [[CrossRef](#)]
43. Xu, F.; Mei, J.; Zheng, M.; Bai, D.; Wu, D.; Gao, Z.; Jiang, K. Au nanoparticles modified branched TiO₂ nanorod array arranged with ultrathin nanorods for enhanced photoelectrochemical water splitting. *J. Alloy. Compd.* **2017**, *693*, 1124–1132. [[CrossRef](#)]
44. Chang, Y.; Xu, J.; Zhang, Y.; Ma, S.; Xin, L.; Zhu, L.; Xu, C. Optical Properties and Photocatalytic Performances of Pd Modified ZnO Samples. *J. Phys. Chem. C* **2009**, *113*, 18761–18767. [[CrossRef](#)]
45. Tri, P.N.; Nguyen, T.A.; Nguyen, T.H.; Carriere, P. Antibacterial Behavior of Hybrid Nanoparticles (Chapter 7). In *Noble Metal-Metal Oxide Hybrid Nanoparticles: Fundamentals and Applications*; Mohapatra, S., Nguyen, T.H., Nguyen-Tri, P., Eds.; Elsevier: Amsterdam, The Netherlands, 2019; pp. 141–155. [[CrossRef](#)]
46. Standard and White LED Basics and Operation. Available online: <https://www.maximintegrated.com/en/app-notes/index.mvp/id/3070> (accessed on 10 June 2019).
47. Reyes-Coronado, D.; Gattorno, G.R.; E Espinosa-Pesqueira, M.; Cab, C.; De Coss, R.; Oskam, G. Phase-pure TiO₂ nanoparticles: Anatase, brookite and rutile. *Nanotechnology* **2008**, *19*. [[CrossRef](#)]
48. Alshamsi, H.A.H.; Hussein, B.S. Hydrothermal Preparation of Silver Doping Zinc Oxide Nanoparticles: Studys, Characterization and Photocatalytic Activity. *Orient. J. Chem.* **2018**, *34*, 1898–1907. [[CrossRef](#)]
49. Anandalakshmi, K.; Venugobal, J.; Ramasamy, V. Characterization of silver nanoparticles by green synthesis method using Pedalium murex leaf extract and their antibacterial activity. *Appl. Nanosci.* **2016**, *6*, 399–408. [[CrossRef](#)]
50. Kuriakose, S.; Choudhary, V.; Satpati, B.; Mohapatra, S.; Xu, R. Enhanced photocatalytic activity of Ag–ZnO hybrid plasmonic nanostructures prepared by a facile wet chemical method. *Beilstein J. Nanotechnol.* **2014**, *5*, 639–650. [[CrossRef](#)]

51. Kuriakose, S.; Choudhary, V.; Satpati, B.; Mohapatra, S. Facile synthesis of Ag-ZnO hybrid nanospindles for highly efficient photocatalytic degradation of methyl orange. *Phys. Chem. Chem Phys.* **2014**, *16*, 17560–17568. [[CrossRef](#)] [[PubMed](#)]
52. Tian, Y.; Tatsuma, T. Plasmon-induced photoelectrochemistry at metal nanoparticles supported on nanoporous TiO₂. *Chem. Commun.* **2004**, *16*, 1810. [[CrossRef](#)] [[PubMed](#)]
53. Cai, R.; Hashimoto, K.; Itoh, K.; Kubota, Y.; Fujishima, A. Photokilling of malignant cells with ultrafine TiO₂ powder. *Bull. Chem. Soc. Jpn.* **1991**, *64*, 1268–1273. [[CrossRef](#)]
54. Ubonchonlakate, K.; Sikong, L.; Saito, F. Photocatalytic disinfection of P. aeruginosa bacterial Ag-doped TiO₂ film. *Procedia Eng.* **2012**, *32*, 656–662. [[CrossRef](#)]
55. Sakthivel, S.; Shankar, M.; Palanichamy, M.; Arabindoo, B.; Bahnemann, D.; Murugesan, V. Enhancement of photocatalytic activity by metal deposition: Characterisation and photonic efficiency of Pt, Au and Pd deposited on TiO₂ catalyst. *Water Res.* **2004**, *38*, 3001–3008. [[CrossRef](#)] [[PubMed](#)]
56. Yue, L.; Wang, Q.; Zhang, X.; Wang, Z.; Xia, W.; Dong, Y. Synthesis of Ag/TiO₂ Core/Shell Nanoparticles with Antibacterial Properties. *Bull. Korean Chem. Soc.* **2011**, *32*, 2607–2610. [[CrossRef](#)]
57. Dhanalekshmi, K.I.; Meen, K.S.; Ramesh, I. Synthesis and Characterization of Ag@TiO₂ Core-shell nanoparticles and study of its antibacterial activity. *Int. J. Nanotechnol. Appl.* **2013**, *3*, 5–14.
58. Zhang, H.; Chen, G. Potent Antibacterial Activities of Ag/TiO₂ Nanocomposite Powders Synthesized by a One-Pot Sol–Gel Method. *Environ. Sci. Technol.* **2009**, *43*, 2905–2910. [[CrossRef](#)]
59. Hidayati, N.; Barudin, A.; Sreekantan, S.; Thong, O.M.; Sahgal, G. Antibacterial Activity of Ag-TiO₂ Nanoparticles with Various Silver Contents. *Mater. Sci. Forum* **2013**, *756*, 238–245.
60. Jin, T.; Sun, D.; Su, J.Y.; Zhang, H.; Sue, H.J. Antimicrobial Efficacy of Zinc Oxide Quantum Dots against Listeria monocytogenes, Salmonella Enteritidis, and Escherichia coli O157:H7. *J. Food Sci.* **2009**, *74*, M46–M52. [[CrossRef](#)]
61. Kumar, K.M.; Mandal, B.K.; Naidu, E.A.; Sinha, M.; Kumar, K.S.; Reddy, P.S. Synthesis and Characterization of Flower Shaped Zinc Oxide Nanostructures and Its Antimicrobial Activity. *Spectrochim. Acta Part A* **2013**, *104*, 171–174. [[CrossRef](#)]
62. Lipovsky, A.; Nitzan, Y.; Gedanken, A.; Lubart, R. Antifungal activity of ZnO nanoparticles—The role of ROS mediated cell injury. *Nanotechnology* **2011**, *22*, 105101. [[CrossRef](#)]
63. Stoimenov, P.K.; Klinger, R.L.; Marchin, G.L.; Klabunde, K.J. Metal Oxide Nanoparticles as Bactericidal Agents. *Langmuir* **2002**, *18*, 6679–6686. [[CrossRef](#)]
64. Ibănescu, M.; Muşat, V.; Textor, T.; Badilita, V.; Mahltig, B. Photocatalytic and antimicrobial Ag/ZnO nanocomposites for functionalization of textile fabrics. *J. Alloy. Compd.* **2014**, *610*, 244–249. [[CrossRef](#)]
65. Nagaraju, G.; Udayabhanu; Shivaraj; Prashanth, S.A.; Shastri, M.; Yathish, K.V.; Anupama, C.; Rangappa, D. Electrochemical heavy metal detection, photocatalytic, photoluminescence, biodiesel production and antibacterial activities of Ag–ZnO nanomaterial. *Mater. Res. Bull.* **2017**, *94*, 54–63. [[CrossRef](#)]
66. Wei, Y.; Chong, Y.B.; Du, H.; Kong, J.; He, C. Loose Yarn of Ag-ZnO-PAN/ITO Hybrid Nanofibres: Preparation, Characterization and Antibacterial Evaluation. *Mater. Des.* **2018**, *139*, 153–161. [[CrossRef](#)]
67. Phuong, N.-T.; Rtimi, S. Claudiane Ouellet Plamondon. In *Nanomaterials Based Coatings: Fundamentals and Applications*; Elsevier: Amsterdam, The Netherlands, 2019; ISBN 9780128158845.
68. Tri, P.N.; Guinault, A.; Sollogoub, C. Élaboration et propriétés des composites polypropylène recyclé/fibres de bambou. *Matériaux Tech.* **2012**, *100*, 413–423.
69. Azizi, S.; David, E.; Fréchette, M.F.; Nguyen-Tri, P.; Ouellet-Plamondon, C.M. Electrical and thermal conductivity of ethylene vinyl acetate composite with graphene and carbon black filler. *Polym. Test.* **2018**, *72*, 24–31. [[CrossRef](#)]
70. Azizi, S.; David, E.; Fréchette, M.F.; Nguyen-Tri, P.; Ouellet-Plamondon, C.M. Electrical and thermal phenomena in low-density polyethylene/carbon black composites near the percolation threshold. *J. Appl. Polym. Sci.* **2018**, *136*, 47043. [[CrossRef](#)]
71. Boukehili, H.; Tri, P.N. Helium gas barrier and water absorption behavior of bamboo fiber reinforced recycled polypropylene. *J. Reinf. Plast. Compos.* **2012**, *31*, 1638–1651. [[CrossRef](#)]
72. Phuong, N.T.; Gilbert, V. Non-isothermal Crystallization Kinetics of Short Bamboo Fiber-reinforced Recycled Polypropylene Composites. *J. Reinf. Plast. Compos.* **2010**, *29*, 2576–2591. [[CrossRef](#)]
73. Phuong, N.T.; Sollogoub, C.; Guinault, A. Relationship between fiber chemical treatment and properties of recycled pp/bamboo fiber composites. *J. Reinf. Plast. Compos.* **2010**, *29*, 3244–3256. [[CrossRef](#)]

74. Tri, P.N.; Rtimi, S.; Nguyen, T.A.; Vu, M.T. Physics, Electrochemistry, Photochemistry, and Photoelectrochemistry of Hybrid Nanoparticles. In *Noble Metal-Metal Oxide Hybrid Nanoparticles*; Woodhead Publishing: Sawston, UK, 2019; pp. 95–123.
75. Tri, P.N.; Ouellet-Plamondon, C.; Rtimi, S.; Assadi, A.A.; Nguyen, T.A. Methods for Synthesis of Hybrid Nanoparticles. In *Noble Metal-Metal Oxide Hybrid Nanoparticles*; Woodhead Publishing: Sawston, UK, 2019; pp. 51–63.
76. Nguyen, T.V.; Tri, P.N.; Nguyen, T.D.; El Aidani, R.; Trinh, V.T.; Decker, C. Accelerated degradation of water borne acrylic nanocomposites used in outdoor protective coatings. *Polym. Degrad. Stab.* **2016**, *128*, 65–76. [[CrossRef](#)]
77. Tri, P.N.; Prud'Homme, R.E. Crystallization and Segregation Behavior at the Submicrometer Scale of PCL/PEG Blends. *Macromolecules* **2018**, *51*, 7266–7727.
78. Nguyen, T.P. Nanoscale analysis of the photodegradation of Polyester fibers by AFM-IR. *J. Photochem. Photobiol. A Chem.* **2018**, *371*, 196–204. [[CrossRef](#)]
79. Tri, P.N.; Prud'homme, R.E. Nanoscale Lamellar Assembly and Segregation Mechanism of Poly(3-hydroxybutyrate)/Poly(ethylene glycol) Blends. *Macromolecules* **2018**, *51*, 181–188. [[CrossRef](#)]
80. El Aidani, R.; Nguyen-Tri, P.; Malajati, Y.; Lara, J.; Vu-Khanh, T. Photochemical aging of an e-PTFE/NOMEX[®] membrane used in firefighter protective clothing. *Polym. Degrad. Stab.* **2013**, *98*, 1300–1310. [[CrossRef](#)]
81. Zeb, G.; Tri, P.N.; Le, X.T.; Palacin, S. Pulse potential deposition of thick polyvinylpyridine-like film on the surface of titanium nitride. *RSC Adv.* **2016**, *6*, 80825–80829. [[CrossRef](#)]
82. Nguyen, T.V.; Le, X.H.; Dao, P.H.; Decker, C.; Nguyen-Tri, P. Stability of acrylic polyurethane coatings under accelerated aging tests and natural outdoor exposure: The critical role of the used photo-stabilizers. *Prog. Org. Coat.* **2018**, *124*, 137–146. [[CrossRef](#)]
83. Nguyen-Tri, P.; Nguyen, T.H.; Ouellet Plamondon, C.; Vo Dai-Viet, N.; Nanda, S.; Mishra, A.; Chao, H.P.; Bajpai, A.K. Recent Progress in the Preparation, Properties and Applications of Superhydrophobic Nano-based Coatings and Surfaces: A review. *Prog. Org. Coat.* **2019**, *132*, 235–256. [[CrossRef](#)]
84. Nguyen-Tri, P.; Altiparmak, F.; Nguyen, N.; Tuduri, L.; Ouellet-Plamondon, C.M.; Prud'Homme, R.E. Robust Superhydrophobic Cotton Fibers Prepared by Simple Dip-Coating Approach Using Chemical and Plasma-Etching Pretreatments. *ACS Omega* **2019**, *4*, 7829–7837. [[CrossRef](#)]
85. Nguyen-Tri, P.; Triki, E.; Nguyen, T.A. Butyl Rubber-Based Composite: Thermal Degradation and Prediction of Service Lifetime. *J. Compos. Sci.* **2019**, *3*, 48. [[CrossRef](#)]
86. Nguyen-Tri, P.; Nguyen, T.A.; Carriere, P.; Xuan, C.N. Nanocomposite Coatings: Preparation, Characterization, Properties, and Applications. *Int. J. Corros.* **2018**, *2018*, 4749501. [[CrossRef](#)]



© 2019 by the authors. Licensee MDPI, Basel, Switzerland. This article is an open access article distributed under the terms and conditions of the Creative Commons Attribution (CC BY) license (<http://creativecommons.org/licenses/by/4.0/>).